

Discovery and Identification of Small Molecules as Methuosis Inducers with In Vivo Antitumor Activities

Wei Huang, Xihuan Sun, Yunzhan Li, Zhixiang He, Li Li, Zhou Deng, Xiaoxing Huang, Shang Han, Ting Zhang, Jiaji Zhong, Zheng Wang, Qingyan Xu, Jianming Zhang, and Xianming Deng

J. Med. Chem., **Just Accepted Manuscript** • DOI: 10.1021/acs.jmedchem.8b00753 • Publication Date (Web): 07 Jun 2018

Downloaded from <http://pubs.acs.org> on June 7, 2018

Just Accepted

"Just Accepted" manuscripts have been peer-reviewed and accepted for publication. They are posted online prior to technical editing, formatting for publication and author proofing. The American Chemical Society provides "Just Accepted" as a service to the research community to expedite the dissemination of scientific material as soon as possible after acceptance. "Just Accepted" manuscripts appear in full in PDF format accompanied by an HTML abstract. "Just Accepted" manuscripts have been fully peer reviewed, but should not be considered the official version of record. They are citable by the Digital Object Identifier (DOI®). "Just Accepted" is an optional service offered to authors. Therefore, the "Just Accepted" Web site may not include all articles that will be published in the journal. After a manuscript is technically edited and formatted, it will be removed from the "Just Accepted" Web site and published as an ASAP article. Note that technical editing may introduce minor changes to the manuscript text and/or graphics which could affect content, and all legal disclaimers and ethical guidelines that apply to the journal pertain. ACS cannot be held responsible for errors or consequences arising from the use of information contained in these "Just Accepted" manuscripts.



Discovery and Identification of Small Molecules as Methuosis Inducers with *In Vivo* Antitumor Activities

Wei Huang,^{†, ‡, #} Xihuan Sun,^{†, ‡, #} Yunzhan Li,^{†, ‡} Zhixiang He,^{†, ‡} Li Li,^{†, ‡} Zhou Deng,^{†, ‡}
Xiaoxing Huang,^{†, ‡} Shang Han,^{†, ‡} Ting Zhang,^{†, ‡}, Jiayi Zhong,^{†, ‡, §} Zheng Wang,^{†, ‡} Qingyan
Xu,^{†, ‡} Jianming Zhang,[⊥] Xianming Deng^{*, †, ‡}

[†]State Key Laboratory of Cellular Stress Biology, Innovation Center for Cell Signaling Network,
School of Life Sciences, Xiamen University, Xiamen, Fujian 361102, China.

[‡]State-province Joint Engineering Laboratory of Targeted Drugs from Natural Products, Xiamen
University, Xiamen, Fujian 361102, China.

[§]Medical College of Xiamen University, Xiamen, Fujian 361102, China.

[⊥]Cutaneous Biology Research Center, Massachusetts General Hospital, Harvard Medical School,
Boston, MA 02129, USA.

ABSTRACT: Methuosis is a novel nonapoptotic mode of cell death characterized by vacuole
accumulation in the cytoplasm. In this report, we describe a series of azaindole-based
compounds that cause vacuolization in MDA-MB-231 cells. The most potent vacuole-inducer,

1
2
3
4 compound **13** (Cmpd. 13), displayed differential cytotoxicities against a broad panel of cancer
5
6
7 cell lines, such as MDA-MB-231, A375, HCT116, and MCF-7, but it did not inhibit the growth
8
9
10 of the nontumorigenic epithelial cell line MCF-10A. A mechanism study confirmed that the cell
11
12 death was caused by inducing methuosis. Furthermore, Cmpd. 13 exhibited substantial
13
14 pharmacological efficacy in the suppression of tumor growth in a xenograft mouse model of
15
16 MDA-MB-231 cells without apparent side effects, which makes this compound the first example
17
18 of a methuosis inducer with potent *in vivo* efficacy. These results demonstrate that methuosis
19
20 inducers might serve as novel therapeutics for the treatment of cancer.
21
22
23
24
25
26
27
28
29
30
31
32
33
34
35
36
37
38
39
40
41
42
43
44
45
46
47
48
49
50
51
52
53
54
55
56
57
58
59
60

INTRODUCTION

Despite an increasing number of clinically available anticancer agents, intrinsic or acquired resistance remains a great challenge in both chemotherapy and targeted therapy.¹ Several mechanisms have been implicated in drug resistance, including increases in drug efflux² or DNA repair capacity³ or altering apoptotic pathways.⁴⁻⁵ As many therapeutic agents work by triggering intrinsic apoptosis,⁶ the discovery of alternative cell death pathways to kill these apoptotic resistant tumor cells is of great interest.

Several nonapoptotic cell death mechanisms,⁷⁻⁸ as exemplified by autophagy⁹ and necrosis,¹⁰ have been described. Recently, a new type of nonapoptotic cell death was named methuosis, which is characterized by vacuole accumulation in the cytoplasm.¹¹⁻¹² These vacuoles are derived from macropinocytotic vesicles showing impaired trafficking and recycling. As a result, decreased metabolic activity and rupture of the cell membrane eventually lead to cell death. Although the precise molecular mechanism is not clear,¹³⁻¹⁴ several methuosis inducers have been reported. For example, indole-based chalcones such as MOMIPP (**1**) can effectively cause methuosis in glioblastoma U251 cells.¹⁵⁻¹⁹ Moreover, MOMIPP showed similar activities against both temozolomide-sensitive and temozolomide-resistant U251 cells. A quinoline derivative named Vacquinol-1 (**2**) also induces methuosis in glioblastomas.²⁰ Recently, a ursolic acid derivative (**3**) was reported to display cytostatic properties via methuosis against several cancer cell lines with IC₅₀ values of approximately 15 μ M.²¹ However, no *in vivo* pharmacological data

have been reported for these methuosis inducers. To understand the pharmacological efficacy of methuosis inducers as anticancer agents, we report the discovery and identification of small molecule Cmpd. 13 as a potent *in vitro* methuosis inducer. More importantly, Cmpd. 13 exhibits a remarkable tumor-suppressing effect in a xenograft mouse model, making this compound the first example of a methuosis inducer with potent *in vivo* efficacy.

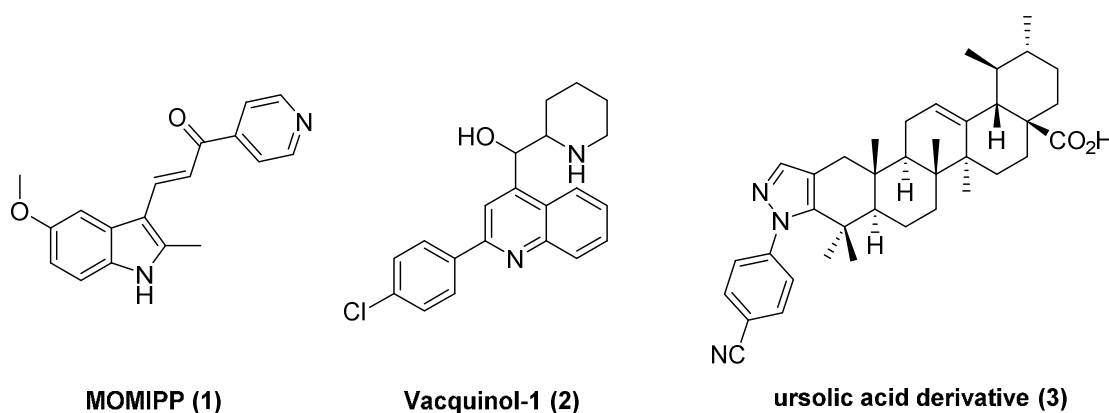


Figure 1. Structures of reported methuosis inducers.

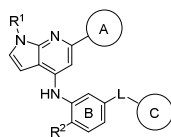
RESULTS

Discovery of compound 13 with potent antitumor activity. As part of a large-scale screen for bioactive small molecules for cancer therapy, compound **12** caught our attention because it effectively caused dramatic cytoplasmic vacuolization in MDA-MB-231 cells at a concentration of 10 μ M. However, the vacuolization effect caused by compound **12** decreased in a dose-dependent manner to a negligible level at 1 μ M. To obtain more potent vacuolization inducers, we started a systematic structure-activity relationship (SAR) study using MOMIPP as a

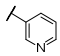
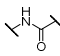
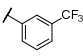
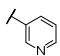
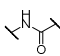
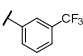
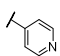
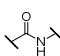
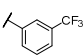
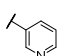
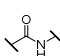
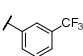
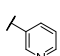
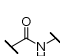
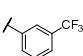
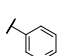
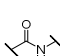
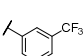
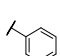
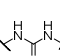
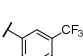
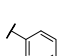
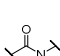
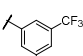
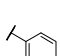
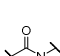
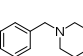
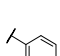
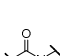
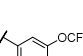
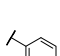
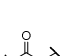
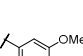
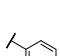
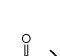
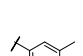
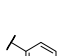
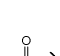
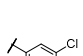
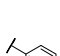
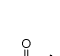
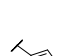
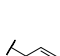
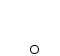
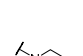
positive control (Table 1). First, the functionality of the A ring was explored. Replacing the pyridin-4-yl moiety with a pyridin-3-yl afforded compound **13**, which induced extensive vacuolization even at a low concentration of 1 μ M (Figure S1). However, replacement of the pyridin-4-yl moiety with phenyl, substituted phenyl, furan-3-yl or thiophen-3-yl moieties had severe adverse effects. Almost no vacuolization could be observed when the cells were treated with compounds **14–18**, even at 10 μ M. These data suggest that there are key interactions occurring between the pyridin-3-yl fragment and its target(s). Then, minor modifications of the pyrrole unit of the scaffold were made. The methylated derivative, compound **19**, dramatically decreased vacuolization at 1 μ M. Next, we turned our attention to the aniline substituent at the 4-position of this scaffold. Compound **20**, which lacked the *o*-methyl substituent on the B ring, showed a similar level of activity. When the orientation of the amide bond (linker **L**) was reversed, resulting compounds **21–24** showed vacuole-inducing capabilities at 10 μ M that were similar to those of their counterparts **12**, **13**, **19** and **20**, respectively. However, only compound **22** retained its activity at 1 μ M. The thiourea linkage-containing derivative, compound **25**, also lost its vacuole-inducing activity at 1 μ M. Therefore, we decided to modify the C ring based on the structure of compound **22**. The addition of a hydrophobic group and a hydrophilic group at the meta-position resulted in compounds **26** and **27**, respectively, which induced less vacuole formation, even at 10 μ M. Replacing the trifluoromethyl group with trifluoromethoxy, methoxy, methyl, and chloro groups resulted in compounds **28–31**, which showed various degrees of activity at 1 μ M. The pyrazole-substituted derivative, compound **32**, was a potent

vacuole-inducer at 10 μM but was inactive at 1 μM . Compound **33**, which possessed a morpholine substituent, completely lost activity. The SAR exploration of 4,6-disubstituted aza-indoles revealed that a free hydrogen ($\text{R}^1 = \text{H}$), pyridin-3-yl (A ring), and 3-trifluoromethyl phenyl (C ring) groups were key structural features required to achieve potent vacuole-inducing activity. The most active compound **13** (Cmpd. 13) induced greater than 99% vacuolization in cells, even at 1 μM .

Table 1. Structure-activity Relationship Study of 4,6-Disubstituted Aza-indoles



Cmpd	R^1	R^2	A ring	L	C ring	Vacuolization ratio (%) ^a	
						1 μM	10 μM
12	H	Me				1.46 \pm 1.37	96.34 \pm 1.10
13	H	Me				99.75 \pm 0.56	100.00
14	H	Me				0.00	0.00
15	H	Me				0.27 \pm 0.6	1.63 \pm 0.69
16	H	Me				0.03 \pm 0.07	0.33 \pm 0.67
17	H	Me				0.24 \pm 0.53	0.00
18	H	Me				0.00	0.21 \pm 0.29

19	Me	Me				16.08±3.26	96.27±2.50
20	H	H				96.61±2.21	98.98±0.76
21	H	Me				0.00	1.94±2.13
22	H	Me				70.29±11.52	99.42±0.86
23	Me	Me				3.63±1.11	70.96±15.72
24	H	H				3.78±0.95	80.23±7.52
25	H	Me				1.26±0.92	87.3±6.45
26	H	Me				0.00	0.00
27	H	Me				0.62±0.87	0.00
28	H	Me				38.57±8.58	99.66±0.77
29	H	Me				76.86±10.97	100.00
30	H	Me				11.24±2.24	97.68±1.49
31	H	Me				19.49±2.97	96.75±1.24
32	H	Me				2.48±1.11	95.24±1.44
33	H	Me				0.00	0.00
MOMIPP (1)						7.01±1.35	96.47±3.38

^aMDA-MB-231 cells were treated with test compounds at concentrations of 1 μM or 10 μM for 24 h. Five fields of cells were randomly selected and photographed, and then, the percentages of vacuolated cells were quantitated. See EXPERIMENTAL SECTION for details.

Cmpd. 13 was selected for further evaluation of its anticancer activities. As shown in Table 2, Cmpd. 13 showed a broad spectrum of cytotoxicity against a panel of human cancer cell lines with IC_{50} values in the micromolar range. A much lower cytotoxic effect was observed against the nontumorigenic epithelial cell line MCF-10A, representing normal human breast cells, and the observed IC_{50} value was greater than 10 μ M. The antiproliferative activity of Cmpd. 13 was further confirmed in a crystal violet staining assay, which revealed that the survival rate of MDA-MB-231 cells was reduced significantly in a dose-dependent manner (Figure 2B and C). The morphological changes in MDA-MB-231 cells treated with 2 μ M Cmpd. 13 were examined using an optical microscope, which showed that vesicles accumulated and gradually fused to form larger vacuoles after 12 h. Most cells were full of vacuoles after 24 h and lost viability after 48 h (Figure 2D). These data demonstrate that Cmpd. 13 is a potent and selective anticancer agent.

Table 2. IC₅₀ Values of Cmpd. 13 and MOMIPP against Cancer and Normal Cells^a

	Cmpd. 13	MOMIPP
Cell lines	IC ₅₀ (μM)	IC ₅₀ (μM)
A375	0.326±0.026	5.020±0.08
SK-MEL-28	1.370±0.061	8.156±0.247
SK-MEL-30	1.662±0.128	>10
A549	1.892±0.092	>10
MDA-MB-231	1.571±0.066	>10
MDA-MB-435S	2.268±0.100	>10
MCF-7	2.611±0.739	>10
HCT116	1.008±0.042	>10
BGC823	1.566±0.015	>10
HepG2	1.197±0.344	>10
MCF-10A	>10	>10

^aCells were treated with Cmpd. 13 or MOMIPP for 48 h, and viability values were determined by MTS assays.

The IC₅₀ values were calculated by GraphPad Prism 5 and are presented as the means ± SD of triplicate samples.

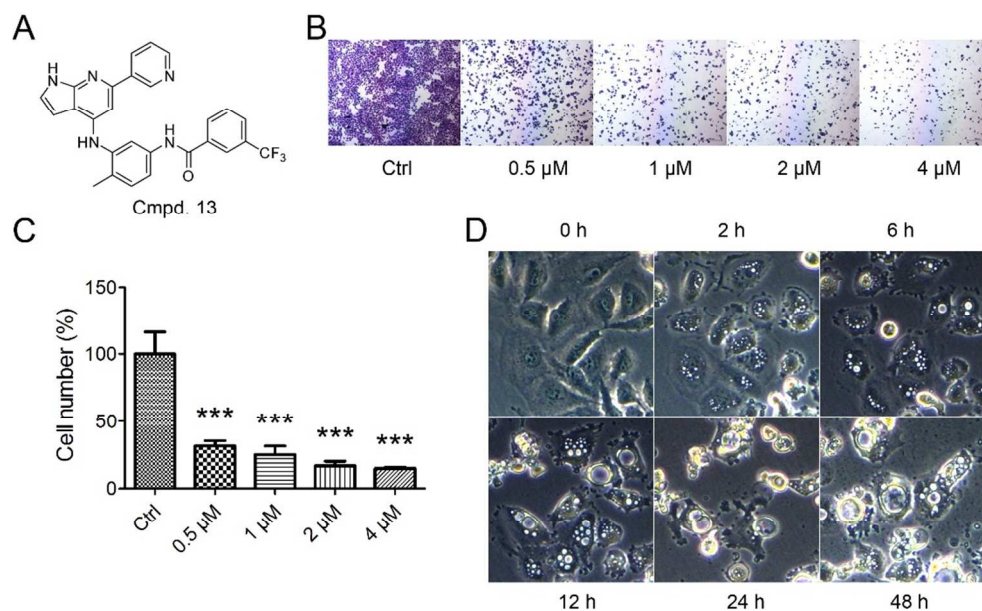


Figure 2. Cmpd. 13 induces extensive vacuolization and reduces the survival rate of MDA-MB-231 cells. (A) Structure of Cmpd. 13. (B) MDA-MB-231 cells were stained with crystal violet after 48 h of incubation with DMSO (control) or Cmpd. 13 at the indicated concentrations. (C) Quantification results for the crystal violet staining. (***) $p < 0.001$ (D) MDA-MB-231 cells were treated with Cmpd. 13 at a concentration of 2 μM, and the morphological changes were observed by optical microscopy at the indicated time.

Identification of Cmpd. 13 as an effective methuosis inducer. As Cmpd. 13 inhibits cancer cell proliferation by inducing full vacuolization in the cytoplasm, we sought to determine if the cell death was caused by methuosis, which is nonapoptotic. Therefore, PARP cleavage and caspase-3 activity were analyzed in MDA-MB-231 cells treated with Cmpd. 13.²² As shown in Figure 3A, cleaved PARP could not be detected after treatment with 0.5 ~ 4 μM Cmpd. 13. The increase in caspase-3 activity was not significant (Figure 3B). Moreover, when cells were

pretreated with Z-VAD-FMK, a pan-caspase inhibitor, for 1 h, neither cell death nor vacuolization could be prevented (Figure 3C and D). Under the same conditions, cells treated with staurosporine (STS) could be significantly rescued by treatment with Z-VAD-FMK (Figure 3C). Additionally, the necrosis inhibitor, necrostatin-1, could not prevent cellular vacuolization or rescue cells from Cmpd. 13 (Figure 3E and F). These results clearly indicate that the cell death caused by Cmpd. 13 is neither apoptosis nor necrosis.

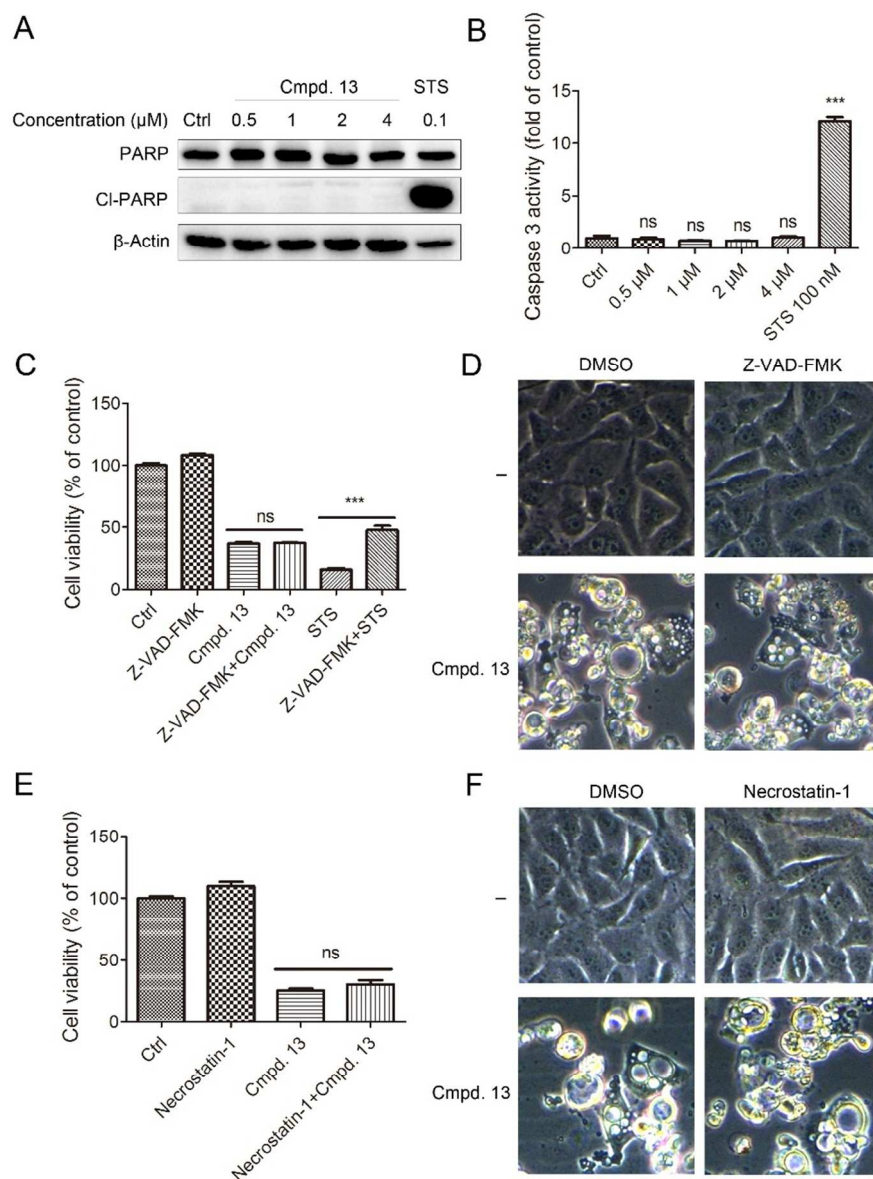


Figure 3. Cell death caused by Cmpd. 13 is distinct from apoptosis or necrosis. (A) MDA-MB-231 cells were treated with DMSO (control), Cmpd. 13 or STS for 24 h at the indicated concentrations. PARP and cleaved PARP were analyzed by Western blot. (B) MDA-MB-231 cells were treated with DMSO (control), Cmpd. 13 or STS for 24 h at the indicated concentrations. The cells were then lysed, and caspase 3 activity was analyzed by a caspase 3 activity kit. (C) MDA-MB-231 cells were treated with DMSO (control), 100 μM Z-VAD-FMK,

2 μM Cmpd. 13, 0.1 μM STS or combinations of these as indicated for 48 h. Viability values were determined
by MTS assays and are presented as the means \pm SD of triplicate samples ($***p < 0.001$). (D) Optical
microscopy images of MDA-MB-231 cells treated with DMSO (control), 100 μM Z-VAD-FMK, 2 μM Cmpd.
13, or their combination for 24 h. (E) MDA-MB-231 cells were treated with DMSO (control), 50 μM
necrostatin-1, 2 μM Cmpd. 13, or their combinations for 48 h. Viability values were determined by MTS
assays and are presented as the means \pm SD of triplicate samples. (F) Optical microscopy images of
MDA-MB-231 cells treated with DMSO (control), 50 μM necrostatin-1, 2 μM Cmpd. 13, or their combination
for 24 h.

Next, we investigated the relationship between Cmpd. 13-induced cell death and autophagy.^{8,}
²³ We first used Western blot analysis to determine whether the autophagosome marker LC3 was
elevated.²⁴ As shown in Figure 4A, LC3-II increased in time- and dose-dependent manners
according to the ratio of LC3-II/ β -Actin, which suggests that Cmpd. 13 disrupts autophagic
flux.²⁵ However, the autophagy inhibitor 3-methyladenine (3-MA) could prevent neither
vacuolization nor cell death in MDA-MB-231 cells treated with Cmpd. 13 (Figure 4B and C),
which excluded autophagy as the cause of cell death induced by Cmpd. 13.

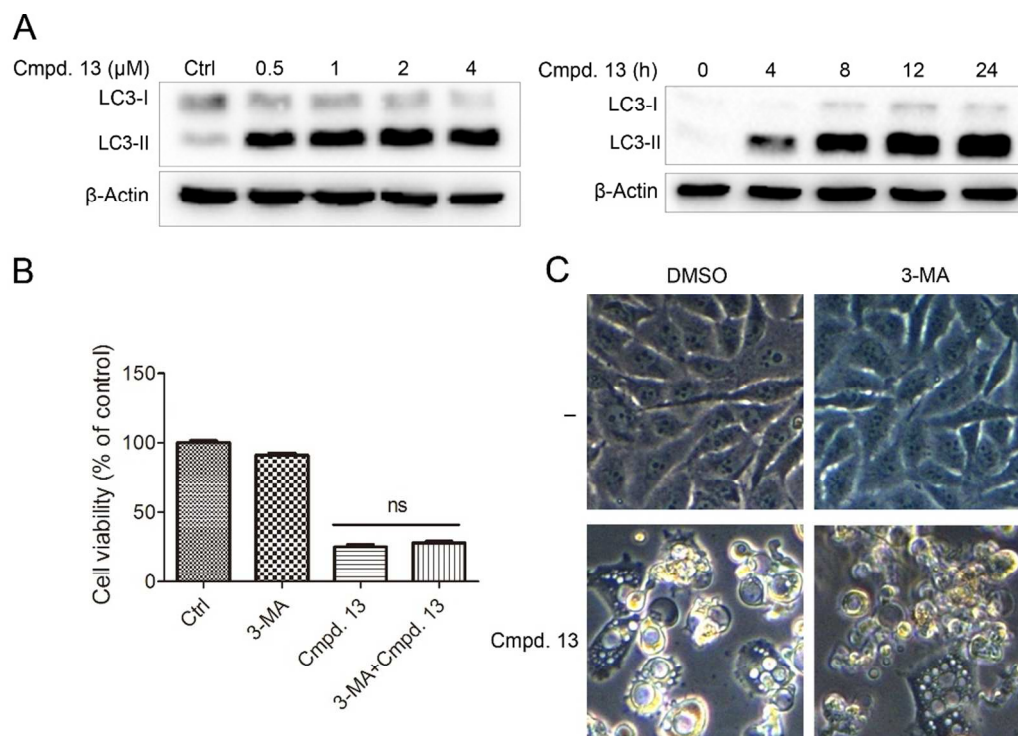


Figure 4. Cell death caused by Cmpd. 13 is distinct from autophagy. (A) MDA-MB-231 cells were treated with DMSO (control) or Cmpd. 13 for 24 h at the indicated concentrations or 2 μM Cmpd. 13 for the indicated time. LC3 was analyzed by Western blot. (B) MDA-MB-231 cells were treated with DMSO (control), 1 mM 3-MA, 2 μM Cmpd. 13, or their combination for 48 h. Viability values were determined by MTS assays and are presented as the means ± SD of triplicate samples. (C) Optical microscopy images of MDA-MB-231 cells treated with DMSO (control), 1 mM 3-MA, 2 μM Cmpd. 13, or their combination for 24 h.

We next turned our attention to the origin of the vacuoles. As shown in Figure 5A and B, neither Mito-tracker nor ER-tracker were incorporated into the vacuoles, suggesting that they did not originate from the mitochondria or endoplasmic reticulum (ER). This conclusion was further confirmed by transmission electron microscopy (Figure 5C), which clearly showed that these

1
2
3
4 organelles remained integrated aside the vacuoles. In methuosis, the vacuoles are derived from
5
6
7 macropinosomes, which fuse with each other and take on some characteristics of late endosomes
8
9
10 but do not merge with lysosomes.^{12, 15} Therefore, we investigated whether the vacuoles induced
11
12 by Cmpd. 13 exhibited the same properties. As shown in Figure 6A, the fluid-phase tracer
13
14 Lucifer yellow (LY) accumulated in most of the vacuoles, which is consistent with what was
15
16
17 observed in macropinocytosis. Furthermore, the late endosomal marker Rab7 was detected on the
18
19
20 membranes of the vacuoles (Figure 6B), but most of the Lyso-tracker did not overlap with these
21
22
23 vacuoles (Figure 6C). Taken together, these observations demonstrated that the vacuoles induced
24
25
26 by Cmpd. 13 possessed the characteristics of methuosis, which suggests that Cmpd. 13 is a
27
28
29 potent methuosis inducer.
30
31
32
33
34
35
36
37
38
39
40
41
42
43
44
45
46
47
48
49
50
51
52
53
54
55
56
57
58
59
60

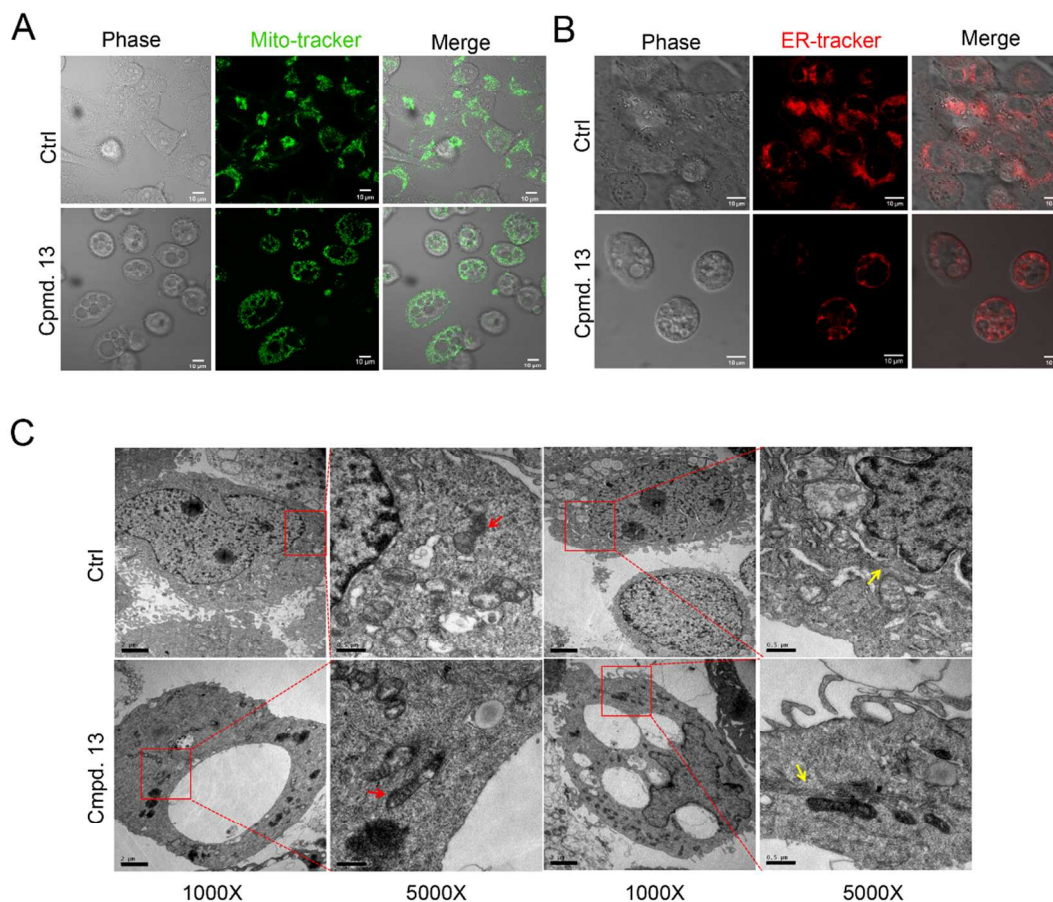


Figure 5. Vacuoles induced by Cmpd. 13 did not originate from the mitochondria or endoplasmic reticulum (ER). (A) Phase-contrast and fluorescent images of MDA-MB-231 cells treated with DMSO (control) or 2 μ M Cmpd. 13 for 12 h and then incubated with Mito-tracker. Scale bar, 10 μ m. (B) Phase-contrast and fluorescent images of MDA-MB-231 cells treated with DMSO (control) or 2 μ M Cmpd. 13 for 12 h and then incubated with ER-tracker. Scale bar, 10 μ m. (C) Electron microscopy images of MDA-MB-231 cells treated with DMSO (control) or 2 μ M Cmpd. 13 for 12 h. Red and yellow arrows indicate that the mitochondria and ER are not swelling. Scale bar, 2 μ m for 1000X, 0.5 μ m for 5000X.

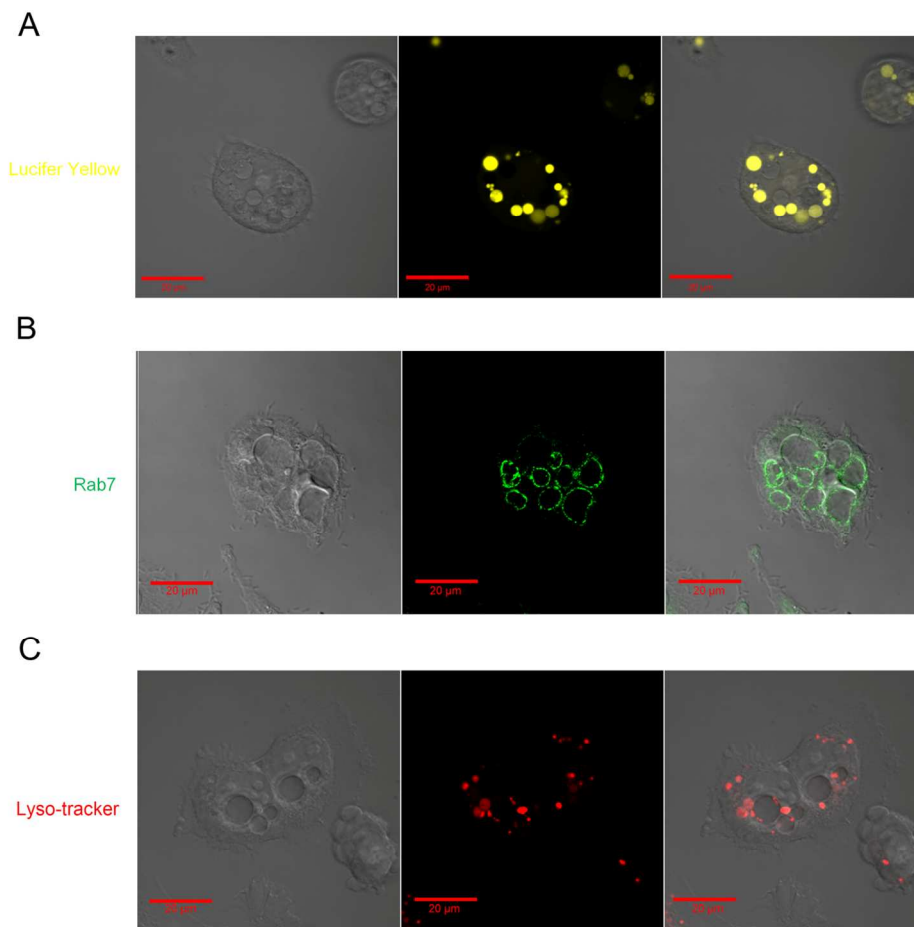


Figure 6. The vacuoles induced by Cmpd. 13 are derived from macropinosomes and take on the characteristics of endosomes but remain distinct from lysosomes. (A) Phase-contrast and fluorescent images of MDA-MB-231 cells treated with 2 μM Cmpd. 13 for 12 h under Lucifer yellow incubation. Scale bar, 20 μm . (B) Phase-contrast and immunofluorescent images of MDA-MB-231 cells treated with 2 μM Cmpd. 13 for 12 h followed by staining with anti-Rab7. Scale bar, 20 μm . (C) Phase-contrast and fluorescent images of MDA-MB-231 cells treated with 2 μM Cmpd. 13 for 12 h and then incubated with Lyso-tracker. Scale bar, 20 μm .

Cmpd. 13 inhibits tumor growth *in vivo*. To extend the potential preclinical application of methuosis inducers, the pharmacokinetics of Cmpd. 13 were assessed in BALB/c mice at a dose of 1 mg/kg via intravenous (IV) injection. Cmpd. 13 was found to have a half-life ($T_{1/2}$) of 8.74 h, a clearance (Cl) of 36.5 mL/min/kg, and a volume of distribution (V_d) of 15.5 L/kg, which represent moderate pharmacokinetic properties. The *in vivo* antitumor efficacy of Cmpd. 13 was further evaluated using triple-negative breast cancer cells (MDA-MB-231 cells) in a mouse xenograft model. As shown in Figure 7, treatment with Cmpd. 13 led to substantial suppression of tumor growth in a dose-dependent manner (Figure 7A and Figure S2), and the tumor growth inhibition (TGI) values were $25.85 \pm 0.30\%$ and $60.15 \pm 0.04\%$ at doses of 5 mg/kg and 20 mg/kg, respectively. In addition, Cmpd. 13 did not cause a significant loss of body weight during treatment. Furthermore, H & E staining showed that numerous vacuoles were visible in drug-treated tumor tissues, indicating that Cmpd. 13 can induce methuosis *in vivo* (Figure 7C). Treatment with Cmpd. 13 on healthy ICR mice at dose of 20 mg/kg for 12 days did not induce vacuoles in normal tissues and had no effects on body weight and blood chemistry (Figure S3). Together, these results demonstrate that Cmpd. 13 inhibits tumor growth *in vivo* with good tolerability.

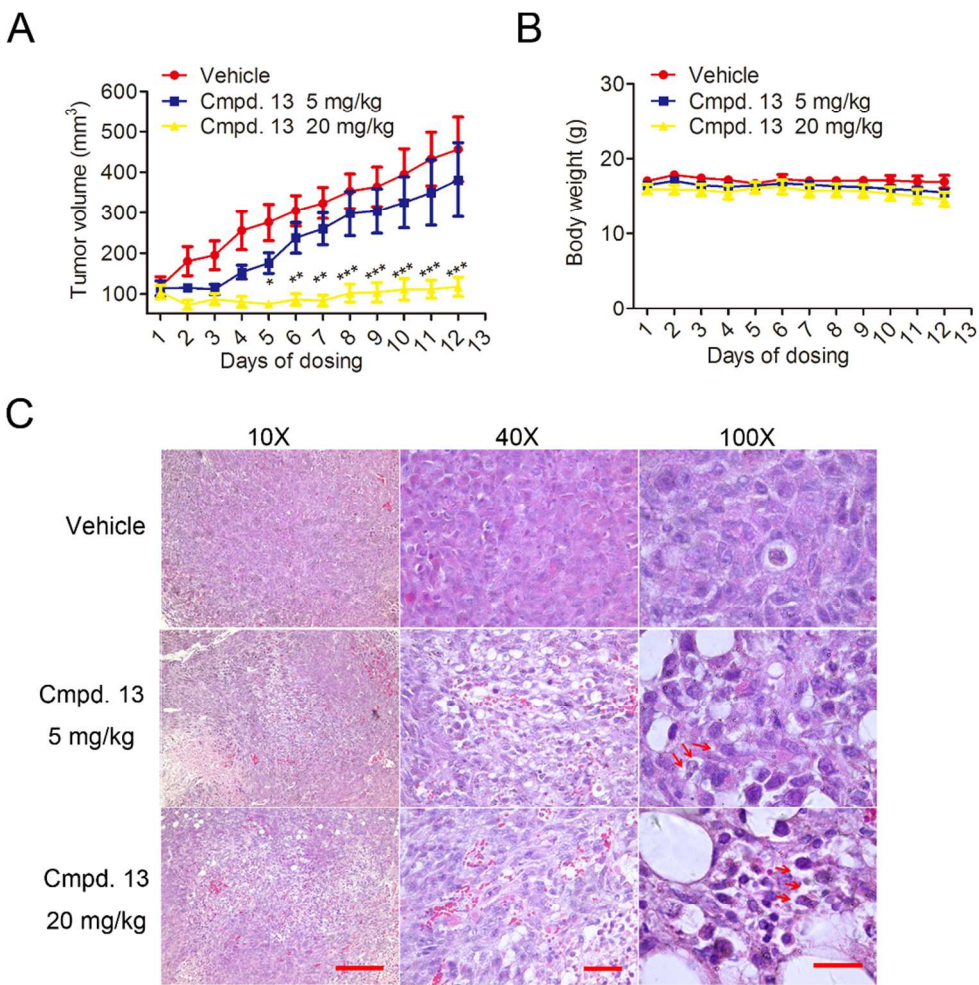
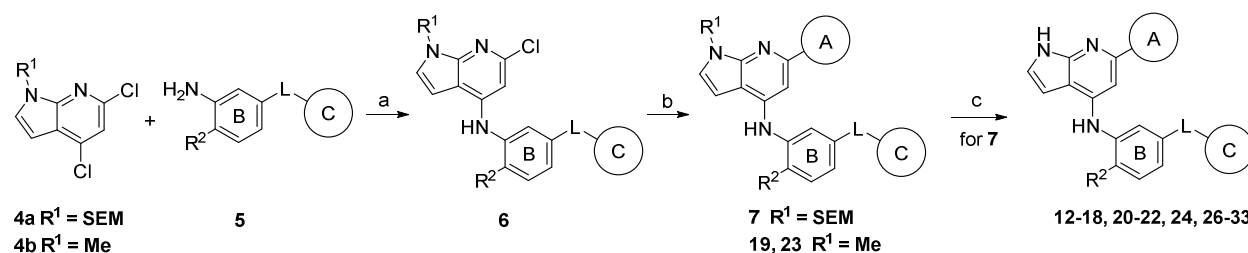


Figure 7. Cmpd. 13 exhibited *in vivo* efficacy in a xenograft mouse model of MDA-MB-231 cells. (A) and (B) Tumor volume and body weight of mice during treatment. Cmpd. 13 was administered intravenously once daily at 5 mg/kg or 20 mg/kg. Tumor volume and body weight were measured every day (* $p < 0.05$, ** $p < 0.01$, *** $p < 0.001$). Error bars indicate mean tumor volume \pm SEM and mean body weight \pm SEM ($n = 6$ animals each group). (C) Hematoxylin-eosin staining (H & E) in tumors untreated or after 12 days of treatment with Cmpd. 13. Red arrows indicate vacuoles. Scale bar, 25 μm for 10X and 100X, 50 μm for 40X.

CHEMISTRY

As shown in Scheme 1, intermediate **6** was obtained from **4** and **5** through Buchwald-Hartwig cross coupling,²⁶⁻²⁷ which gave intermediate **7** or final products **19** and **23** after Suzuki cross coupling with boronic acids.²⁸⁻³⁰ Deprotection of the SEM group furnished final compounds **12-18**, **20-22**, **24** and **26-33**.

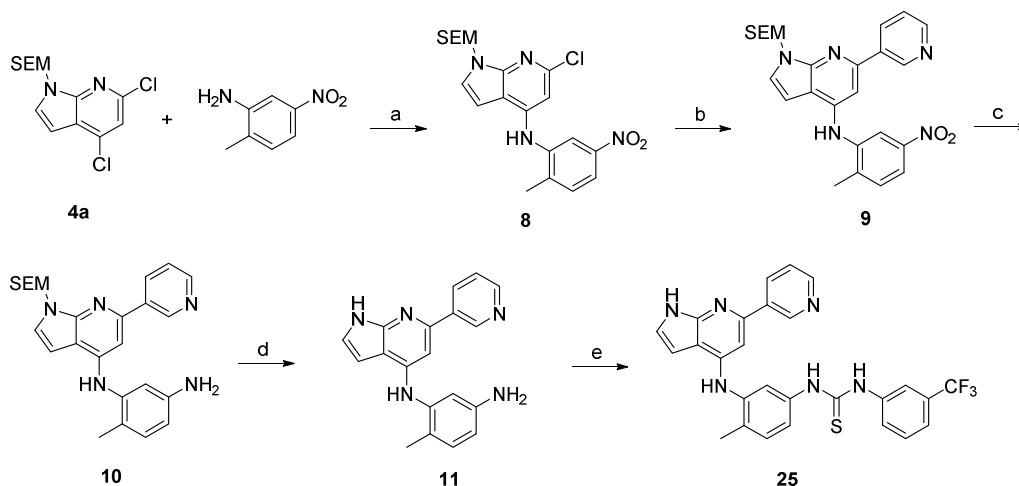
Scheme 1. Synthesis of azaindole-based compounds^a



^aReagents and conditions: a. Xphos, Pd₂(dba)₃, K₂CO₃, *t*-BuOH, 60 °C. b. PdCl₂(dppf)•CH₂Cl₂, Na₂CO₃, 1,4-dioxane/H₂O (V/V = 2/1), 100 °C. c. (1) TFA; (2) MeOH/THF/LiOH (1.0 M, aq.) (V/V/V = 1/1/1).

The synthesis of compound **25** is illustrated in Scheme 2. Intermediate **9** was obtained through Pd-catalyzed cross coupling reactions as described above. After reduction of the nitro group and deprotection of the SEM, resulting aniline **11** was reacted with 1-isothiocyanato-3-(trifluoromethyl)benzene to give compound **25**.

Scheme 2. Synthesis of compound **25**^a



"Reagents and conditions: a. Xphos, $\text{Pd}_2(\text{dba})_3$, K_2CO_3 , *t*-BuOH, 60 °C. b. $\text{PdCl}_2(\text{dppf}) \cdot \text{CH}_2\text{Cl}_2$, Na_2CO_3 , 1,4-dioxane/ H_2O (V/V = 2/1), 100 °C. c. Zn, NH_4Cl (aq.), EtOH, 60 °C. d. (1) TFA; (2) MeOH/THF/LiOH (1.0 M, aq.) (V/V/V = 1/1/1). e. 1-isothiocyanato-3-(trifluoromethyl)benzene, THF, 60 °C.

DISCUSSION AND CONCLUSIONS

Methuosis was first defined in cancer cells with ectopic expression of constitutively activated Ras and was proven to be distinct from necrosis, autophagy and other nonapoptotic forms of cell death.^{12, 31} These characteristics grant methuosis inducers great potential for the treatment of cancers that are resistant to conventional therapies. Indeed, temozolomide-resistant U251 cells remain sensitive to MOMIPP, an indole-based chalcone methuosis inducer.¹⁶ Herein, we reported a series of 4,6-disubstituted aza-indoles that are structurally distinct from existing methuosis inducers. Further structure-activity relationship studies revealed the key factors for methuosis-inducing activity. For example, the pyridin-3-yl moiety at the 2-position of this scaffold and the hydrophobic group at the meta-position of the C ring are critical for activity. A

certain degree of flexibility in the pyrrole motif or B ring exists, which allows further derivatization to improve potency or specificity.

Triple-negative breast cancer (TNBC) accounts for approximately 15% of all breast cancers and has a poor disease prognosis, a high risk of recurrence and a worse disease-free survival rate compared to other subtypes.³² Because TNBC does not express estrogen receptors or progesterone receptors (PRs) and lacks human epidermal growth factor receptor-2 (HER2) amplification, it is insensitive to antihormonal and HER2 targeted therapies.³³⁻³⁴ Currently, surgery and/or cytotoxic chemotherapy are the standard care for the treatment of TNBC, and these methods do not show satisfying outcomes.³⁵ Whether methuosis inducers can show therapeutic benefits *in vivo* is of great interest. Cmpd. 13 induced vacuolization in both cancer cells (MDA-MB-231 cells) and nontumorigenic epithelial cells (MCF-10A cells), and it exhibited differential antiproliferative activities with IC₅₀ values of 1.88 μ M and >10 μ M, respectively. These results indicate that a sufficient therapeutic window may exist among tumor and normal tissues. This hypothesis has been confirmed by the subsequent *in vivo* studies. Data from an MDA-MB-231 xenograft mouse model showed that Cmpd. 13 significantly suppressed tumor growth in a dose-dependent manner, which demonstrates the acceptable therapeutic benefits of this compound. Importantly Cmpd. 13 was tolerated in animals, and a significant decrease in body weight was not observed during treatment. Further studies to identify the cellular target(s) of this series of azaindole-based compounds and to elucidate the detailed

molecular mechanism are needed to extend our understanding of the vulnerability of cancer cells to these methuosis inducers.

Taken together, our results demonstrate that the methuosis inducer Cmpd. 13 is effective and tolerable *in vivo*, and thus, it can serve as a good starting point for the development of methuosis-based therapies against cancers for which there are no targeted therapeutics available, such as TNBC.

EXPERIMENTAL SECTION

General Methods for Chemistry. Reagents and solvents were obtained from commercial sources and were used without further purification. Reactions were monitored by thin layer chromatography (TLC) on glass plates coated with silica gel with fluorescent indicator. Compounds were purified either by chromatography on silica gel or by preparative high performance liquid chromatography (HPLC). Silica gel chromatography was performed on Teledyne ISCO CombiFlash system (RF200) eluting with petroleum ether/ethyl acetate (PE/EA) or dichloromethane/methanol (DCM/MeOH). Preparative HPLC was conducted on Waters autopurification system consisting of a 2767 sample manager, a 2545 binary gradient module, a 2489 UV detector, and a 3100 mass detector [SunFireTM C18 column, 5 μ M, 19 x 50 mm, 10 min linear gradient from 10% solvent A (methanol with 0.035% trifluoroacetic acid) in solvent B (water with 0.035% trifluoroacetic acid) to 100% A, then hold for 4 min at 100% A, 20 mL/min]. NMR spectra were recorded on a Bruker Ultrashield Plus-600 (600 MHz) spectrometer and

chemical shifts are reported in δ (ppm). ^1H chemical shifts are reported as s (singlet), d (doublet), dd (doublet of doublet), t (triplet), q (quartet), m (multiplet), and brs (broad singlet) and are referenced to the residual solvent signal: DMSO- d_6 (2.50), CDCl_3 (7.26). ^{13}C spectra are referenced to the residual solvent signal: DMSO- d_6 (39.52), CDCl_3 (77.16). Mass Spectra were recorded on Waters 3100 Mass Detector. High Resolution Mass Spectra were obtained on Thermo Fisher Scientific LTQ FTICR-MS. The purity of all tested compounds were determined to be > 95% by HPLC with UV detection at 254 nm [Waters LC/MS system, SunFireTM C18 column, 5 μM , 4.6 x 50 mm, a 0.5 min hold at 5% solvent A (methanol with 0.035% trifluoroacetic acid) in solvent B (water with 0.035% trifluoroacetic acid), then a 4 min linear increase to 95% A, then to 100% A in 1 min, then a 4 min hold at 100% A, 1 mL/min].

General procedure. *N*-(3-((6-chloro-1-((2-(trimethylsilyl)ethoxy)methyl)-1*H*-pyrrolo[2,3-*b*]pyridin-4-yl)amino)-4-methylphenyl)-3-(trifluoromethyl)benzamide (**6a**) The mixture of 4,6-dichloro-1-((2-(trimethylsilyl)ethoxy)methyl)-1*H*-pyrrolo[2,3-*b*]pyridine (**4a**, 500 mg, 1.58 mmol), *N*-(3-amino-4-methylphenyl)-3-(trifluoromethyl)benzamide (**5a**, 464 mg, 1.58 mmol), Xphos (56 mg, 0.12 mmol), $\text{Pd}_2(\text{dba})_3$ (72 mg, 0.079 mmol) and K_2CO_3 (654 mg, 4.74 mmol) were stirred in *t*-BuOH (15 mL) at 65 °C for 6 hours under N_2 , then filtered through celite. The filtrate was concentrated and purified by CombiFlash purification system to give **6a** as a colorless oil (540 mg, 59.5%). ^1H NMR (600 MHz, DMSO- d_6) δ 10.50 (s, 1H), 8.76 (s, 1H), 8.29 (s, 1H), 8.26 (d, $J = 7.9$ Hz, 1H), 7.97 (d, $J = 7.8$ Hz, 1H), 7.79 (t, $J = 8.0$ Hz, 1H), 7.77 (d,

$J = 2.1$ Hz, 1H), 7.67 (dd, $J = 8.3, 2.1$ Hz, 1H), 7.37 (d, $J = 8.5$ Hz, 1H), 7.34 (d, $J = 3.6$ Hz, 1H), 6.58 (d, $J = 3.6$ Hz, 1H), 6.03 (s, 1H), 5.49 (s, 2H), 3.55 – 3.50 (m, 2H), 2.18 (s, 3H), 0.87 – 0.81 (m, 2H), -0.07 (s, 9H); ^{13}C NMR (150 MHz, DMSO- d_6) δ 164.5, 148.5, 147.8, 145.8, 138.3, 138.1, 136.2, 132.3, 131.6, 130.4, 130.2, 129.7 (q, $J = 32.0$ Hz), 128.6 (q, $J = 3.5$ Hz), 125.9, 124.7 (q, $J = 3.9$ Hz), 124.5 (q, $J = 272.4$ Hz), 119.1, 118.9, 107.3, 99.7, 97.6, 72.9, 65.7, 17.6, -1.0; MS (ESI) m/z 575 [$\text{C}_{28}\text{H}_{30}\text{ClF}_3\text{N}_4\text{O}_2\text{Si} + \text{H}$] $^+$.

***N*-(4-methyl-3-((6-(pyridin-3-yl)-1-((2-(trimethylsilyl)ethoxy)methyl)-1*H*-pyrrolo[2,3-*b*]pyridin-4-yl)amino)phenyl)-3-(trifluoromethyl)benzamide (7a).** The mixture of **6a** (60 mg, 0.10 mmol), pyridin-3-ylboronic acid (15 mg, 0.12 mmol), Na_2CO_3 (42 mg, 0.40 mmol) and $\text{PdCl}_2(\text{dppf}) \cdot \text{CH}_2\text{Cl}_2$ (8 mg, 0.01 mmol) were stirred in 1,4-dioxane/ H_2O (0.8/0.4 mL) at 100 °C under N_2 for 2 hours, then filtered through celite. The filtrate was concentrated and purified by CombiFlash purification system to give **7a** as a light yellow oil (52.0 mg, 80.8%). ^1H NMR (600 MHz, DMSO- d_6) δ 10.49 (s, 1H), 9.16 (dd, $J = 2.4, 0.9$ Hz, 1H), 8.53 (dd, $J = 4.7, 1.6$ Hz, 1H), 8.50 (s, 1H), 8.30 – 8.27 (m, 2H), 8.25 (d, $J = 7.8$ Hz, 1H), 7.96 – 7.93 (m, 1H), 7.88 (d, $J = 2.2$ Hz, 1H), 7.77 (t, $J = 7.8$ Hz, 1H), 7.58 (dd, $J = 8.3, 2.2$ Hz, 1H), 7.44 (ddd, $J = 8.0, 4.8, 0.8$ Hz, 1H), 7.38 (d, $J = 3.6$ Hz, 1H), 7.35 (d, $J = 8.3$ Hz, 1H), 6.85 (s, 1H), 6.59 (d, $J = 3.6$ Hz, 1H), 5.64 (s, 2H), 3.64 – 3.55 (m, 2H), 2.24 (s, 3H), 0.94 – 0.84 (m, 2H), -0.13 (s, 9H); ^{13}C NMR (150 MHz, DMSO- d_6) δ 164.5, 149.8, 149.3, 149.1, 148.1, 146.9, 139.1, 137.8, 136.2, 136.0, 134.1, 132.2, 131.4, 130.2, 129.6 (q, $J = 32.0$ Hz), 129.5, 128.6 (q, $J = 3.4$ Hz), 126.6, 124.7 (q, $J = 3.9$

Hz), 124.4 (q, $J = 272.5$ Hz), 124.0, 118.3, 118.0, 108.2, 99.6, 96.6, 72.5, 65.8, 17.8, 17.6, -1.0;

MS (ESI) m/z 618 [$C_{33}H_{34}ClF_3N_5O_2Si + H$]⁺.

***N*-(4-methyl-3-((6-(pyridin-3-yl)-1*H*-pyrrolo[2,3-*b*]pyridin-4-yl)amino)phenyl)-3-(trifluoromethyl)benzamide (13).** Compound **7a** (40.0 mg, 0.065 mmol) was stirred in TFA (1 mL) at room temperature for 1 hour. The mixture was concentrated under vacuum and the residue was dissolved in MeOH/THF (1/1 mL). To this solution was added 1 M aqueous LiOH solution (1 mL) and the resulting mixture were stirred at room temperature for another 1 hour before diluting with water (30 mL). Then the mixture were extracted with EtOAc (20 mL × 3) and the combined organic layers were washed with brine, dried over Na₂SO₄, filtered and concentrated under reduced pressure. The residue was purified by CombiFlash purification system to give **13** as a white solid (12.3 mg, 38.9%). ¹H NMR (600 MHz, DMSO-*d*₆) δ 11.51 – 11.48 (m, 1H), 10.48 (s, 1H), 9.11 (d, $J = 2.3$ Hz, 1H), 8.53 (dd, $J = 4.7, 1.6$ Hz, 1H), 8.37 (s, 1H), 8.30 – 8.28 (m, 1H), 8.28 – 8.23 (m, 2H), 7.98 – 7.95 (m, 1H), 7.89 (d, $J = 2.2$ Hz, 1H), 7.78 (t, $J = 7.8$ Hz, 1H), 7.59 (dd, $J = 8.3, 2.2$ Hz, 1H), 7.44 (dd, $J = 8.0, 4.7$ Hz, 1H), 7.35 (d, $J = 8.3$ Hz, 1H), 7.24 (dd, $J = 3.4, 2.4$ Hz, 1H), 6.79 (s, 1H), 6.55 (dd, $J = 3.4, 2.0$ Hz, 1H), 2.26 (s, 3H); ¹³C NMR (150 MHz, DMSO-*d*₆) δ 164.4, 150.5, 149.1, 149.1, 148.1, 146.6, 139.3, 137.8, 136.5, 136.3, 134.1, 132.3, 131.4, 130.2, 129.6 (q, $J = 32.1$ Hz), 129.3, 128.5 (q, $J = 3.9$ Hz), 124.7 (q, $J = 3.9$ Hz), 124.4 (q, $J = 270.1$ Hz), 124.0, 123.3, 118.0, 117.7, 108.2, 99.0, 96.0, 17.8. MS (ESI) m/z 488 [$M + H$]⁺; HRMS (DART): calcd for [$C_{27}H_{20}F_3N_5O + H$]⁺ 488.1693, found 488.1692.

The other intermediates and final compounds were synthesized in similar ways and characterization data are provided in the Supporting Information.

Cell Culture. MDA-MB-231, A375, SK-MEL-28, SK-MEL-30, BGC823, A549, MDA-MB-435S, MCF-7, HCT116, HepG2 were grown in Dulbecco's Modified Eagle Medium (DMEM) or RPMI-1640 medium containing 10% fetal bovine serum, penicillin (100 U/mL) and streptomycin (100 µg/mL). MCF-10A cell line was cultured in F12/RPMI medium containing 5% horse serum, 2 mg/mL insulin, 1 mg/mL hydrocortisone, 100 µg/mL EGF, 100 U/mL penicillin and 100 µg/mL streptomycin. All cell lines were maintained at 37°C in 5% CO₂ humidified air.

Immunoblotting. After compound treatment, cells were harvested and lysed in cell lysis buffer containing 50 mM Tris-HCl (pH 7.5), 150 mM NaCl, 1% (v/v) Triton X-100, 5% glycerol, 1 mM phenylmethylsulfonyl fluoride, 5 µg/mL leupeptin, 1 mM sodium orthovanadate and 50 mM sodium fluoride. Total protein concentrations were measured by BCA analysis (Beyotime, Haimen, China). Equal amounts of protein were loaded for separation by electrophoresis in a 10%-15% SDS-PAGE gel and then electrophoretically transferred to Immobilon-P PVDF membrane (Millipore, Billerica, MA, USA). Proteins were probed with appropriate primary antibodies and peroxidase-conjugated secondary antibodies. The membranes were incubated with enhanced chemiluminescence (ECL) reagents and detected using a ChemiDOC™ XRS+ Imaging system (Bio-Rad, Hercules, CA, USA). Antibodies against PARP,

1
2
3
4 Cl-PARP, LC3 and Rab7 were obtained from Cell Signaling Technology (Beverly, MA, USA).
5

6
7 Anti- β -Actin was purchased from Sigma (St. Louis, MO, USA).
8
9

10 **Caspase 3 Activity Assay.** After treatment as indicated for 24 h, MDA-MB-231 cells were
11
12 harvested and lysed. Caspase 3 activity was detected using caspase 3 activity assay kit according
13
14 to the manufacturer's instructions (Beyotime).
15
16
17

18
19 **Cell Morphology and Viability.** To determine the percentage of cells with cytoplasmic
20
21 vacuoles, phase contrast images of live cells were captured with a Zeiss OBSERVER A1/AX10
22
23 microscope. After treatments for 24 h, five fields of cells were randomly selected and
24
25 photographed. Cells containing one or more phase-lucent vacuoles with diameters $> 3 \mu\text{m}$ or > 3
26
27 smaller vacuoles ($0.5\text{--}3 \mu\text{m}$) were counted as positive. Cell viability was determined by MTS
28
29 assay. Cells were seeded at an appropriate density into 96-well plates and allowed to attach
30
31 overnight. Compounds were serially diluted with growth medium, and then added in triplicate
32
33 into 96-well plates and incubated for 48 h. Subsequently, viability was determined by MTS
34
35 (Promega, Madison, WI, USA), according to the manufacturer's instructions and IC_{50} values
36
37 were calculated by software GraphPad Prism5.
38
39
40
41
42
43
44
45
46

47 **Crystal Violet Staining Assay.** MDA-MB-231 cells were seeded into 6-well-plates and
48
49 cultured for 12 h. Then medium was refreshed and cells were exposed to 0.1% DMSO or
50
51 different concentrations of Cmpd. 13. After 48 h incubation, the cells were fixed with 4% (v/v)
52
53
54
55
56

paraformaldehyde for 15 min at room temperature. Subsequently, the cells were stained with crystal violet and observed by optical microscopy (AX20 OBSERVER A1, Zeiss, Germany).

Live Cell Imaging. Mito-tracker Red, ER-tracker and Lyso-tracker Red were purchased from Beyotime (Haimen, China). Lucifer yellow CH was purchased from Molecular Probes (Eugene, OR). MDA-MB-231 cells were seeded in a 30 mm glass bottom culture dish (NEST Biotechnology, China) and allowed to attach overnight. Cells were treated with 2 μ M Cmpd. 13 for 12 h and then incubated with Mito-Tracker, ER-tracker and Lyso-Tracker Red according to the manufacturer's instructions, respectively. In Lucifer yellow (LY) staining, cells were treated with Cmpd. 13 and LY simultaneously for 12 h, then washed with PBS and photographed. All images were collected with a confocal microscope (Zeiss LSM 780).

Immunofluorescence Staining. Cells seeded on coverslips were fixed with 4% (v/v) paraformaldehyde for 15 min at room temperature and permeabilized with 0.1% Triton X-100 for 20 min, followed by blocked for 30 min at room temperature with 5% BSA. Cells were then incubated for 1 h with anti-Rab7 antibody (1:500 dilution; Cell Signaling Technology). After washing for three times with PBS, the cells were further incubated for another 1 h with secondary antibodies Alexa Fluor 488-conjugated anti-rabbit IgG (Life Technologies). Subsequently, the cells were washed three times with PBS. All images were collected with a confocal microscope (Zeiss LSM 780).

Electron Microscopy. MDA-MB-231 cells were fixed in ice-cold 2.5% glutaraldehyde in 0.1 M PBS (pH 7.4) at 4 °C for 3 h, washed three times with 0.1 M PBS (pH 7.4) and post-fixed in 1% OsO₄ in 0.1 M PBS (pH 7.4) at 4 °C for 2 h. The samples were subsequently dehydrated in an ethanol gradient [30% (v/v) ethanol (15 min), 50% (v/v) ethanol (15 min), 70% (v/v) ethanol (15 min), 90% (v/v) ethanol (15 min) and 100% ethanol (2 × 20 min)] and embedded in Spurr's resin. Ultrathin (70 nm) sections were collected on a copper grid, stained with either uranyl acetate or lead citrate and examined under a JEM2100HC transmission electron microscope.

***In Vivo* Tumor Model.** Female BALB/c nude mice (4-6 weeks) were purchased from Beijing Vital River Laboratory Animal Technology Co., Ltd. (Beijing, China). Xenografts were initiated by subcutaneous injection of MDA-MB-231 cells (5×10⁶ cells per mouse). When tumor size (length×width²×0.5) reached to approximately 100 mm³, mice were randomly assigned into groups and treated by tail vein injection with the vehicle [10% (w/v) Kolliphor HS 15 (Sigma)] in normal saline or Cmpd. 13 formulated in the vehicle at the indicated dose and frequency. At 6 h of post-final dose, mice were euthanized and tumors were separated, weighted and subjected to further analysis. All procedures were performed in compliance with the guidelines from the Institutional Animal Care and Use Committee at Experimental Animal Centre in Xiamen University.

Haematoxylin and Eosin Staining. Tumor tissues were fixed in 4% paraformaldehyde, and embedded in paraffin. Then, 4 μ m thick slices were stained with haematoxylin and eosin and examined by light microscopy (Leica DM4 M).

ASSOCIATED CONTENT

Supporting Information.

The Supporting Information is available free of charge on the ACS Publications website at <http://pubs.acs.org>.

Figures S1–S3, general procedure for the synthesis of anilines, characterization data of the intermediates and compounds **12** and **14–33**, NMR and HRMS spectra, HPLC chromatograms of all the final compounds (PDF)

Molecular formula strings (CSV)

AUTHOR INFORMATION

Corresponding Author

* Phone: (+86)592-2184180; Fax: (+86)592-2181722; E-mail: xmdeng@xmu.edu.cn.

Notes

The authors declare no competing financial interests.

Author Contributions

[#]These authors contributed equally to this work.

ACKNOWLEDGMENTS

This work was supported by grants from the National Key R&D Program and the National Natural Science Foundation of China (No. 2017YFA0504504, 2016YFA0502001, 81422045, U1405223 and 81661138005 to X. Deng, 21402165 to W. Huang, and 81603131 to L. Li), the China's 1000 Young Talents Program to X. Deng, the Fundamental Research Funds for the Central Universities of China (No. 20720160064 to X. Deng, and 20720170067 to L. Li), and the Program of Introducing Talents of Discipline to Universities (111 Project, B12001).

ABBREVIATIONS USED

MOMIPP, (*E*)-3-(5-methoxy-2-methyl-1*H*-indol-3-yl)-1-(pyridin-4-yl)prop-2-en-1-one; PARP, poly (ADP-ribose) polymerase; LC3, microtubule associated protein 1 light chain 3; 3-MA, 3-methyladenine; DMSO, dimethyl sulfoxide; MTS, 3-(4,5-dimethylthiazol-2-yl)-5-(3-carboxymethoxyphenyl)-2-(4-sulfophenyl)-2*H*-tetrazolium, inner salt; SCID, severe combined immune deficiency; Xphos, 2-dicyclohexylphosphino-2',4',6'-triisopropylbiphenyl; Pd₂(dba)₃, tris(dibenzylideneacetone) dipalladium; PdCl₂(dppf)•CH₂Cl₂, 1,1'-bis(diphenylphosphino)ferrocene-palladium (II) dichloride dichloromethane complex.

REFERENCES

(1) Holohan, C.; Van Schaeybroeck, S.; Longley, D. B.; Johnston, P. G., Cancer drug resistance: an evolving paradigm. *Nat. Rev. Cancer* **2013**, *13*, 714-726.

(2) Szakacs, G.; Paterson, J. K.; Ludwig, J. A.; Booth-Genthe, C.; Gottesman, M. M., Targeting multidrug resistance in cancer. *Nat. Rev. Drug Discov.* **2006**, *5*, 219-234.

(3) Bouwman, P.; Jonkers, J., The effects of deregulated DNA damage signalling on cancer chemotherapy response and resistance. *Nat. Rev. Cancer* **2012**, *12*, 587-598.

(4) Lowe, S. W.; Cepero, E.; Evan, G., Intrinsic tumour suppression. *Nature* **2004**, *432*, 307-315.

(5) Debatin, K. M.; Krammer, P. H., Death receptors in chemotherapy and cancer. *Oncogene* **2004**, *23*, 2950-2966.

(6) Hurley, L. H., DNA and its associated processes as targets for cancer therapy. *Nat. Rev. Cancer* **2002**, *2*, 188-200.

(7) Galluzzi, L.; Vitale, I.; Abrams, J. M.; Alnemri, E. S.; Baehrecke, E. H.; Blagosklonny, M. V.; Dawson, T. M.; Dawson, V. L.; El-Deiry, W. S.; Fulda, S.; Gottlieb, E.; Green, D. R.; Hengartner, M. O.; Kepp, O.; Knight, R. A.; Kumar, S.; Lipton, S. A.; Lu, X.; Madeo, F.; Malorni, W.; Mehlen, P.; Nunez, G.; Peter, M. E.; Piacentini, M.; Rubinsztein, D. C.; Shi, Y.; Simon, H. U.; Vandenabeele, P.; White, E.; Yuan, J.; Zhivotovsky, B.; Melino, G.; Kroemer, G.,

Molecular definitions of cell death subroutines: recommendations of the Nomenclature Committee on Cell Death 2012. *Cell Death Differ.* **2012**, *19*, 107-120.

(8) Lockshin, R. A.; Zakeri, Z., Apoptosis, autophagy, and more. *Int. J. Biochem. Cell Biol.* **2004**, *36*, 2405-2419.

(9) Levine, B.; Klionsky, D. J., Development by Self-Digestion: Molecular Mechanisms and Biological Functions of Autophagy. *Dev. Cell* **2004**, *6*, 463-477.

(10) Vandenabeele, P.; Galluzzi, L.; Vanden Berghe, T.; Kroemer, G., Molecular mechanisms of necroptosis: an ordered cellular explosion. *Nat. Rev. Mol. Cell Biol.* **2010**, *11*, 700-714.

(11) Chi, S.; Kitanaka, C.; Noguchi, K.; Mochizuki, T.; Nagashima, Y.; Shirouzu, M.; Fujita, H.; Yoshida, M.; Chen, W.; Asai, A.; Himeno, M.; Yokoyama, S.; Kuchino, Y., Oncogenic Ras triggers cell suicide through the activation of a caspase-independent cell death program in human cancer cells. *Oncogene* **1999**, *18*, 2281-2290.

(12) Overmeyer, J. H.; Kaul, A.; Johnson, E. E.; Maltese, W. A., Active ras triggers death in glioblastoma cells through hyperstimulation of macropinocytosis. *Mol. Cancer Res.* **2008**, *6*, 965-977.

(13) Maltese, W. A.; Overmeyer, J. H., Methuosis Nonapoptotic Cell Death Associated with Vacuolization of Macropinosome and Endosome Compartments. *Am. J. Pathol.* **2014**, *184*, 1630-1642.

(14) Maltese, W. A.; Overmeyer, J. H., Non-apoptotic cell death associated with perturbations of macropinocytosis. *Front Physiol.* **2015**, *6*, 38.

(15) Overmeyer, J. H.; Young, A. M.; Bhanot, H.; Maltese, W. A., A chalcone-related small molecule that induces methuosis, a novel form of non-apoptotic cell death, in glioblastoma cells.

Mol. Cancer **2011**, *10*, 69.

(16) Robinson, M. W.; Overmeyer, J. H.; Young, A. M.; Erhardt, P. W.; Maltese, W. A., Synthesis and evaluation of indole-based chalcones as inducers of methuosis, a novel type of nonapoptotic cell death. *J. Med. Chem.* **2012**, *55*, 1940-1956.

(17) Trabbic, C. J.; Dietsch, H. M.; Alexander, E. M.; Nagy, P. I.; Robinson, M. W.; Overmeyer, J. H.; Maltese, W. A.; Erhardt, P. W., Differential Induction of Cytoplasmic Vacuolization and Methuosis by Novel 2-Indolyl-Substituted Pyridinylpropenones. *ACS Med. Chem. Lett.* **2014**, *5*, 73-77.

(18) Trabbic, C. J.; Overmeyer, J. H.; Alexander, E. M.; Crissman, E. J.; Kvale, H. M.; Smith, M. A.; Erhardt, P. W.; Maltese, W. A., Synthesis and biological evaluation of indolyl-pyridinyl-propenones having either methuosis or microtubule disruption activity. *J. Med. Chem.* **2015**, *58*, 2489-2512.

(19) Trabbic, C. J.; George, S. M.; Alexander, E. M.; Du, S.; Offenbacher, J. M.; Crissman, E. J.; Overmeyer, J. H.; Maltese, W. A.; Erhardt, P. W., Synthesis and biological evaluation of isomeric methoxy substitutions on anti-cancer indolyl-pyridinyl-propenones: Effects on potency and mode of activity. *Eur. J. Med. Chem.* **2016**, *122*, 79-91.

(20) Sander, P.; Mostafa, H.; Soboh, A.; Schneider, J. M.; Pala, A.; Baron, A. K.; Moepps, B.; Wirtz, C. R.; Georgieff, M.; Schneider, M., Vacquinol-1 inducible cell death in glioblastoma

multiforme is counter regulated by TRPM7 activity induced by exogenous ATP. *Oncotarget* **2017**, *8*, 35124-35137.

(21) Sun, L.; Li, B.; Su, X.; Chen, G.; Li, Y.; Yu, L.; Li, L.; Wei, W., An Ursolic Acid Derived Small Molecule Triggers Cancer Cell Death through Hyperstimulation of Macropinocytosis. *J. Med. Chem.* **2017**, *60*, 6638-6648.

(22) Boulares, A. H.; Yakovlev, A. G.; Ivanova, V.; Stoica, B. A.; Wang, G.; Iyer, S.; Smulson, M., Role of poly(ADP-ribose) polymerase (PARP) cleavage in apoptosis. Caspase 3-resistant PARP mutant increases rates of apoptosis in transfected cells. *J. Biol. Chem.* **1999**, *274*, 22932-22940.

(23) Marino, G.; Niso-Santano, M.; Baehrecke, E. H.; Kroemer, G., Self-consumption: the interplay of autophagy and apoptosis. *Nat. Rev. Mol. Cell Biol.* **2014**, *15*, 81-94.

(24) Kimura, S.; Noda, T.; Yoshimori, T., Dissection of the autophagosome maturation process by a novel reporter protein, tandem fluorescent-tagged LC3. *Autophagy* **2007**, *3*, 452-460.

(25) Mizushima, N.; Yoshimori, T.; Levine, B., Methods in mammalian autophagy research. *Cell* **2010**, *140*, 313-326.

(26) Paul, F.; Patt, J.; Hartwig, J. F., Palladium-catalyzed formation of carbon-nitrogen bonds. Reaction intermediates and catalyst improvements in the hetero cross-coupling of aryl halides and tin amides. *J. Am. Chem. Soc.* **1994**, *116*, 5969-5970.

(27) Wolfe, J. P.; Wagaw, S.; Buchwald, S. L., An improved catalyst system for aromatic carbon-nitrogen bond formation: The possible involvement of bis(phosphine) palladium complexes as key intermediates. *J. Am. Chem. Soc.* **1996**, *118*, 7215-7216.

(28) Miyaura, N.; Suzuki, A., Stereoselective synthesis of arylated (E)-alkenes by the reaction of alk-1-enylboranes with aryl halides in the presence of palladium catalyst. *J. Chem. Soc., Chem. Commun.* **1979**, 866-867.

(29) Miyaura, N.; Suzuki, A., Palladium-Catalyzed Cross-Coupling Reactions of Organoboron Compounds. *Chem. Rev.* **1995**, *95*, 2457-2483.

(30) Miyaura, N.; Yamada, K.; Suzuki, A., A new stereospecific cross-coupling by the palladium-catalyzed reaction of 1-alkenylboranes with 1-alkenyl or 1-alkynyl halides. *Tetrahedron Lett.* **1979**, *20*, 3437-3440.

(31) Bhanot, H.; Young, A. M.; Overmeyer, J. H.; Maltese, W. A., Induction of nonapoptotic cell death by activated Ras requires inverse regulation of Rac1 and Arf6. *Mol. Cancer Res.* **2010**, *8*, 1358-1374.

(32) Lund, M. J.; Trivers, K. F.; Porter, P. L.; Coates, R. J.; Leyland-Jones, B.; Brawley, O. W.; Flagg, E. W.; O'Regan, R. M.; Gabram, S. G.; Eley, J. W., Race and triple negative threats to breast cancer survival: a population-based study in Atlanta, GA. *Breast Cancer Res. Treat* **2009**, *113*, 357-370.

(33) Foulkes, W. D.; Smith, I. E.; Reis-Filho, J. S., Triple-negative breast cancer. *N. Engl. J. Med.* **2010**, *363*, 1938-1948.

(34) Oakman, C.; Viale, G.; Di Leo, A., Management of triple negative breast cancer. *Breast* **2010**, *19*, 312-321.

(35) Andre, F.; Zielinski, C. C., Optimal strategies for the treatment of metastatic triple-negative breast cancer with currently approved agents. *Ann. Oncol.* **2012**, *23*, vi46-51.

Table of Contents Graphic

